Available online at www.sciencedirect.com
ScienceDirect
C. R. Mecanique 335 (2007) 536–547
COMPTES RENDUS MECANIQUE
http://france.elsevier.com/direct/CRAS2B/

Boussinesq equation, elasticity, beams, plates

From Boussinesq–Love contact to impact between hyperelastic bodies

Zhi-Qiang Feng [a,*], Claude Vallée [b]

[a] *Laboratoire de mécanique et d'énergétique d'Évry, Université d'Évry – Val d'Essonne, 40, rue du Pelvoux, 91020 Évry, France*
[b] *Laboratoire de mécanique des solides, Université de Poitiers, boulevard Marie et Pierre Curie, BP 30179, 86960 Futuroscope, France*

Received 4 December 2006; accepted after revision 17 January 2007

Available online 14 September 2007

Abstract

This article is devoted to the modeling of finite deformations of hyperelastic bodies under contact/impact conditions. A total Lagrangian formulation is adopted to describe the geometrically nonlinear behavior. A first order algorithm is applied to integrate the equations of motion. The contact problem is solved by the bi-potential method. For the finite element implementation, an explicit expression of the tangent operator for the **3é** hyperelastic model is derived. The classical Boussinesq–Love contact problem is first investigated numerically. A second example concerns the impact between two hyperelastic bodies in three-dimension. ***To cite this article: Z.-Q. Feng, C. Vallée, C. R. Mecanique 335 (2007).***

Résumé

Sur le contact de Boussinesq–Love et l'impact entre corps hyperélastiques. Cet article est consacré à la modélisation de grandes déformations hyperélastiques en présence du contact et de l'impact. Une formulation en Lagrangien total est adoptée pour décrire le comportement avec non linéarités géométriques. Un schéma du premier ordre est appliqué pour intégrer les équations du mouvement. Le problème du contact est résolu à l'aide de la méthode du bi-potentiel. Pour l'implantation par éléments finis, une expression explicite de l'opérateur tangent est proposée dans le cas du modèle hyperélastique **3é**. Le problème classique du contact de Boussinesq–Love est traité numériquement. Un deuxième exemple concerne l'impact entre deux blocs hyperélastiques en trois dimensions. ***Pour citer cet article : Z.-Q. Feng, C. Vallée, C. R. Mecanique 335 (2007).***

Keywords: Computational solid mechanics; Isotropic elasticity; Contact–impact

Mots-clés : Mécanique des solides numérique ; Elasticité isotrope ; Contact–impact

1. Introduction

Problems involving contact and friction are among the most difficult ones to solve in mechanics and they are at the same time of practical importance in many engineering branches, as described in the book by Johnson [1]. A large

* Corresponding author.
E-mail addresses: feng@iup.univ-evry.fr (Z.-Q. Feng), vallee@lms.univ-poitiers.fr (C. Vallée).

1631-0721/$ – see front matter
doi:10.1016/j.crme.2007.01.009

number of algorithms for solving contact problems by the finite element method have been presented in the literature. See for example the monographs by Kikuchi and Oden [2], Zhong [3], Wriggers [4], Laursen [5] and the references therein. De Saxcé and Feng [6] have proposed a bi-potential method combined with an augmented Lagrangian formulation. Feng et al. [7] have successfully applied this method to the modeling of static contact problems between Blatz–Ko hyperelastic bodies.

Regarding the time integration for implicit dynamic analysis in structural mechanics, the most commonly used schemes are the second-order schemes such as Newmark, Wilson-θ, HHT [8]. A first order time scheme has also been proposed by Jean [9] for time stepping in granular mechanics. Recently, Feng et al. [10,11] and Magnain [12] have applied this scheme for the modeling of impact problems between elastic and hyperelastic bodies.

Many industrial applications are concerned by foam-like or rubber-like materials. The tire technology is for example one of the main application fields of rubber-like shells. Such materials are also used to improve the performance of safety glass by using interlayers to join the splinters in the case of a crash [13]. In nonlinear elasticity, there exist many constitutive laws describing the hyperelastic behavior of foam-like or rubber-like materials [14–20]. These models are available in many modern commercial finite element codes. In 1999, Lainé, Vallée and Fortuné [21] have proposed a new third-order hyperelastic model, referred here as the **3é** model. The aim of the present paper is to propose a finite element implementation of this model, in view of application to contact/impact problems involving large displacements and large strains. The classical contact problem proposed by Boussinesq [22] and Love [23,24] is first investigated numerically in order to show the validity of the model developed. A second example consists of the impact of two hyperelastic blocks. Both frictionless and frictional contacts are considered to highlight the physical energy dissipation by frictional effects.

2. Hyperelastic bodies and the 3é model

It is well known that, in case of small linear elastic strains, the Hooke law links the Cauchy stress $\boldsymbol{\sigma}$ to the infinitesimal strain $\boldsymbol{\varepsilon}$ by

$$\boldsymbol{\sigma} = 2\mu\boldsymbol{\varepsilon} + \lambda\,\mathrm{tr}(\boldsymbol{\varepsilon})\mathbf{I} \tag{1}$$

where μ and λ are Lamé coefficients. Nonlinear elasticity generalizes the Hooke law by adding supplementary terms as

$$\boldsymbol{\sigma} = 2\mu\boldsymbol{\varepsilon} + \lambda\,\mathrm{tr}(\boldsymbol{\varepsilon})\mathbf{I} + \text{terms in } \boldsymbol{\varepsilon}^2 + \text{terms in } \boldsymbol{\varepsilon}^3 + \cdots \tag{2}$$

Rubber-like materials are usually supposed to be hyperelastic and they often undergo large deformations. To describe the geometrical transformations in the 3D space, the deformation gradient tensor is introduced by

$$\mathbf{F} = \mathbf{I} + \nabla\mathbf{u} = \mathbf{I} + \frac{\partial\mathbf{u}}{\partial\mathbf{x}} \tag{3}$$

where $\mathbf{I}$ is the identity tensor, $\mathbf{x}$ is the position vector and $\mathbf{u}$ is the displacement vector. The constraint of incompressibility (isochoric deformation) corresponds to transformations satisfying to [15]

$$J = \det(\mathbf{F}) = 1 \tag{4}$$

Due to large deformations and large rotations, Green–Lagrange strain is adopted for the nonlinear relationships between strains and displacements. We denote by $\mathbf{C}$ the stretch tensor (or right Cauchy–Green strain tensor): $\mathbf{C} = \mathbf{F}^{\mathrm{T}}\mathbf{F}$. The Green–Lagrange strain tensor $\mathbf{E}$ and its distortional part $\mathbf{E}_d$ are defined as

$$\mathbf{E} = \frac{1}{2}(\mathbf{C} - \mathbf{I}), \qquad \mathbf{E}_d = \mathbf{E} - \frac{\mathrm{tr}(\mathbf{E})}{3}\mathbf{I} \tag{5}$$

For an hyperelastic law, the existence of an elastic potential function W (or strain energy density function) is assumed. It is a scalar function of one of the strain tensors and its derivative with respect to one strain component determines the corresponding stress component. For example

$$\mathbf{S} = \frac{\partial W}{\partial\mathbf{E}} = 2\frac{\partial W}{\partial\mathbf{C}} \tag{6}$$

where $\mathbf{S}$ is the second Piola–Kirchhoff stress tensor. In particular, for isotropic hyperelasticity [16], Eq. (6) can be written as

$$\mathbf{S} = 2\left[I_3 \frac{\partial W}{\partial I_3}\mathbf{C}^{-1} + \left(\frac{\partial W}{\partial I_1} + I_1 \frac{\partial W}{\partial I_2}\right)\mathbf{I} - \frac{\partial W}{\partial I_2}\mathbf{C}\right] \tag{7}$$

where I_i $(i = 1, 2, 3)$ denote the three invariants of the right Cauchy–Green deformation tensor $\mathbf{C}$:

$$I_1 = \operatorname{tr}(\mathbf{C}), \qquad I_2 = \left[I_1^2 - \operatorname{tr}\left(\mathbf{C}^2\right)\right]/2, \qquad I_3 = \det(\mathbf{C}) = J^2 \tag{8}$$

The **3é** constitutive law, proposed by Lainé, Vallée and Fortuné in 1999 [21], describes isotropic compressible or incompressible rubber-like materials. This model is based on the following main ideas:

- If the constitutive law relating $\mathbf{E}$ and $\mathbf{S}$ is isotropic, the strain tensor $\mathbf{E}$ has the same eigenvectors as the stress tensor $\mathbf{S}$.
- The eigenvalues of stress and strain tensors are sorted in the same order: the eigenvector associated to the highest eigenvalue of the stress tensor is also associated to the highest eigenvalue of the strain tensor, etc.

New invariants of $\mathbf{S}$: (X, Y, Z) and $\mathbf{E}$: (x, y, z) are thus introduced as follows:

$$X = \sqrt{\operatorname{tr}(\mathbf{S}_d)^2}\cos\psi, \qquad Y = \sqrt{\operatorname{tr}(\mathbf{S}_d)^2}\sin\psi, \qquad Z = \frac{\operatorname{tr}(\mathbf{S})}{\sqrt{3}} \tag{9}$$

$$x = \sqrt{\operatorname{tr}(\mathbf{E}_d)^2}\cos\vartheta, \qquad y = \sqrt{\operatorname{tr}(\mathbf{E}_d)^2}\sin\vartheta, \qquad z = \frac{\operatorname{tr}(\mathbf{E})}{\sqrt{3}} \tag{10}$$

The so-called Lode's angles (ranging from 0 to $\pi/3$) are defined by

$$\psi = \frac{1}{3}\cos^{-1}\left[3\sqrt{6}\frac{\det(\mathbf{S}_d)}{[\operatorname{tr}(\mathbf{S}_d)^2]^{3/2}}\right], \qquad \vartheta = \frac{1}{3}\cos^{-1}\left[3\sqrt{6}\frac{\det(\mathbf{E}_d)}{[\operatorname{tr}(\mathbf{E}_d)^2]^{3/2}}\right] \tag{11}$$

The choice of the invariants is such that

$$\operatorname{tr}(\mathbf{ES}) = xX + yY + zZ = E_1S_1 + E_2S_2 + E_3S_3 \tag{12}$$

where E_i and S_i $(i = 1, 2, 3)$ stand respectively for the eigenvalues of $\mathbf{E}$ and $\mathbf{S}$ sorted in decreasing order. The Cardan's formula leads to

$$\begin{aligned}
S_1 &= \frac{\operatorname{tr}(\mathbf{S})}{3} + \sqrt{\frac{2}{3}}\sqrt{\operatorname{tr}(\mathbf{S}_d)^2}\cos\psi \\
S_2 &= \frac{\operatorname{tr}(\mathbf{S})}{3} + \sqrt{\frac{2}{3}}\sqrt{\operatorname{tr}(\mathbf{S}_d)^2}\cos\left(\frac{2\pi}{3} - \psi\right) \\
S_3 &= \frac{\operatorname{tr}(\mathbf{S})}{3} + \sqrt{\frac{2}{3}}\sqrt{\operatorname{tr}(\mathbf{S}_d)^2}\cos\left(\frac{2\pi}{3} + \psi\right)
\end{aligned} \tag{13}$$

$$\begin{aligned}
E_1 &= \frac{\operatorname{tr}(\mathbf{E})}{3} + \sqrt{\frac{2}{3}}\sqrt{\operatorname{tr}(\mathbf{E}_d)^2}\cos\vartheta \\
E_2 &= \frac{\operatorname{tr}(\mathbf{E})}{3} + \sqrt{\frac{2}{3}}\sqrt{\operatorname{tr}(\mathbf{E}_d)^2}\cos\left(\frac{2\pi}{3} - \vartheta\right) \\
E_3 &= \frac{\operatorname{tr}(\mathbf{E})}{3} + \sqrt{\frac{2}{3}}\sqrt{\operatorname{tr}(\mathbf{E}_d)^2}\cos\left(\frac{2\pi}{3} + \vartheta\right)
\end{aligned} \tag{14}$$

In view of Eqs. (9), (10), (13), (14), we obtain a linear relationship between the eigenvalues of $\mathbf{S}$ (resp. $\mathbf{E}$) and the invariants of $\mathbf{S}$ (resp. $\mathbf{E}$):

$$\begin{Bmatrix} S_1 \\ S_2 \\ S_3 \end{Bmatrix} = \begin{bmatrix} \frac{2}{\sqrt{6}} & 0 & \frac{1}{\sqrt{3}} \\ \frac{-1}{\sqrt{6}} & \frac{1}{\sqrt{2}} & \frac{1}{\sqrt{3}} \\ \frac{-1}{\sqrt{6}} & \frac{-1}{\sqrt{2}} & \frac{1}{\sqrt{3}} \end{bmatrix} \begin{Bmatrix} X \\ Y \\ Z \end{Bmatrix}, \qquad \begin{Bmatrix} E_1 \\ E_2 \\ E_3 \end{Bmatrix} = \begin{bmatrix} \frac{2}{\sqrt{6}} & 0 & \frac{1}{\sqrt{3}} \\ \frac{-1}{\sqrt{6}} & \frac{1}{\sqrt{2}} & \frac{1}{\sqrt{3}} \\ \frac{-1}{\sqrt{6}} & \frac{-1}{\sqrt{2}} & \frac{1}{\sqrt{3}} \end{bmatrix} \begin{Bmatrix} x \\ y \\ z \end{Bmatrix} \tag{15}$$

The fourth-order strain energy density function expressed in terms of the new invariants of the strain tensor is

$$W(x,y,z)=\left(G+\frac{a_3}{4}z^2\right)\left(x^2+y^2\right)+\frac{3K}{2}z^2+\frac{a_1}{3}\left(x^3-3xy^2\right)+\frac{a_2}{3}z^3+\frac{a_4}{4}z^4+\frac{a_5}{4}\left(x^2+y^2\right)^2 \tag{16}$$

where G is the shear modulus, K the bulk modulus and a_i $(i=1,\ldots,5)$ are parameters of the model. The potential is convex and differentiable if the parameters are such that

$$a_3\geqslant 0,\quad a_4\geqslant 0,\quad a_5\geqslant 0,\quad \sqrt{2Ga_5}\geqslant a_1\geqslant -\sqrt{2Ga_5},\quad 3\sqrt{Ka_4}\geqslant a_2\geqslant -3\sqrt{Ka_4} \tag{17}$$

In this work, we suppose an uncoupling between spherical and distortional parts of $\mathbf{E}$, i.e., $a_3=0$.

From Eq. (6), a simple relationship arises between the chosen invariants of $\mathbf{E}$ and $\mathbf{S}$:

$$X=\frac{\partial W}{\partial x},\qquad Y=\frac{\partial W}{\partial y},\qquad Z=\frac{\partial W}{\partial z} \tag{18}$$

It is pointed out by Criscione [25] that this approach is experimentally tractable since the response terms are mutually orthogonal.

It is noted that for $a_i=0$, we recover the well-known Saint Venant–Kirchhoff strain-energy density

$$W(x,y,z)=\frac{3K}{2}z^2+G\left(x^2+y^2\right)=\frac{K}{2}(\operatorname{tr}\mathbf{E})^2+G\operatorname{tr}(\mathbf{E}_d)^2 \tag{19}$$

By deriving the energy density (16) with respect to the strain tensor, it yields

$$\mathbf{S}=z\left(3K+a_2z+a_4z^2\right)\frac{\mathbf{I}}{\sqrt{3}}+\left[2G+\frac{a_5}{2}\left(x^2+y^2\right)\right]\mathbf{E}_d+\sqrt{6}a_1\left[(\mathbf{E}_d)^2-\frac{x^2+y^2}{3}\mathbf{I}\right] \tag{20}$$

The Cauchy stress (or true stress) tensor $\boldsymbol{\sigma}$ is calculated from the second Piola–Kirchhoff stress tensor $\mathbf{S}$ by the formula:

$$\boldsymbol{\sigma}=\frac{1}{J}\mathbf{F}\mathbf{S}\mathbf{F}^{\mathrm{T}} \tag{21}$$

To construct the tangent stiffness matrix for the analysis of nonlinear structures by the finite element method, one has to determine the stress–strain tangent operator $\mathbb{D}$, which is a fourth-order tensor resulting from the derivation of $\mathbf{S}$ with respect to $\mathbf{E}$ in Eq. (20):

$$\begin{aligned}\mathbb{D}=\frac{\partial\mathbf{S}}{\partial\mathbf{E}}&=\left[K+\frac{2a_2}{3\sqrt{3}}\operatorname{tr}(\mathbf{E})+\frac{a_4}{3}\operatorname{tr}(\mathbf{E})^2\right]\mathbf{I}\otimes\mathbf{I}\\&+\left[2G+\frac{a_5}{2}\operatorname{tr}(\mathbf{E}_d)^2\right]\left(\mathbf{I}\,\overline{\underline{\otimes}}\,\mathbf{I}-\frac{1}{3}\mathbf{I}\otimes\mathbf{I}\right)+a_5\mathbf{E}_d\otimes\mathbf{E}_d\\&+\sqrt{6}a_1\left(\mathbf{I}\,\underline{\otimes}\,\mathbf{E}_d+\mathbf{E}_d\,\underline{\otimes}\,\mathbf{I}-\frac{2}{3}\mathbf{E}_d\otimes\mathbf{I}-\frac{2}{3}\mathbf{I}\otimes\mathbf{E}_d\right)\end{aligned} \tag{22}$$

The coordinate-free symbols $\otimes$, $\underline{\otimes}$ and $\overline{\underline{\otimes}}$ used above are related to the corresponding index symbols in the following way:

$$(\mathbf{A}\otimes\mathbf{B})_{ijkl}=A_{ij}B_{kl},\qquad(\mathbf{A}\,\underline{\otimes}\,\mathbf{B})_{ijkl}=A_{ik}B_{jl},\qquad(\mathbf{A}\,\overline{\underline{\otimes}}\,\mathbf{B})_{ijkl}=\frac{1}{2}(A_{ik}B_{jl}+A_{il}B_{jk}) \tag{23}$$

3. Finite element formulation of nonlinear structures

3.1. Total Lagrangian formulation

In the case of dynamic multibody contact problems with large deformations of hyperelastic solids, the nonlinear relationship between strains and displacements cannot be ignored. The total Lagrangian formulation is adopted in this work to describe nonlinear behavior. It is well known that the strain tensor $\mathbf{E}$ and the stress tensor $\mathbf{S}$ are both symmetric. Thus, we note hereafter $\mathbf{E}$ and $\mathbf{S}$ in vector form as

$$\mathbf{E}=\langle E_{11}\quad E_{22}\quad E_{33}\quad 2E_{12}\quad 2E_{13}\quad 2E_{23}\rangle^{\mathrm{T}},\qquad \mathbf{S}=\langle S_{11}\quad S_{22}\quad S_{33}\quad S_{12}\quad S_{13}\quad S_{23}\rangle^{\mathrm{T}} \tag{24}$$

In the context of the finite element method and with Eq. (3) and Eq. (5), the Green–Lagrange strain can be formally written with linear and nonlinear contributions in terms of nodal displacements [19]:

$$\mathbf{E} = \left(\mathbf{B}_L + \frac{1}{2}\mathbf{B}_{NL}(\mathbf{u})\right)\mathbf{u} \tag{25}$$

where $\mathbf{B}_L$ is the matrix which relates the linear part of the strain term to the nodal displacements, and $\mathbf{B}_{NL}(\mathbf{u})$, the matrix which relates the nonlinear strain term to the nodal displacements. From Eq. (25), the incremental form of the strain-displacement relationship is

$$\delta\mathbf{E} = \big(\mathbf{B}_L + \mathbf{B}_{NL}(\mathbf{u})\big)\delta\mathbf{u} \tag{26}$$

According to the principle of virtual displacement, the virtual work

$$\delta U = \delta\mathbf{u}^{\mathrm{T}}\mathbf{M}\ddot{\mathbf{u}} + \delta\mathbf{u}^{\mathrm{T}}\mathbf{A}\dot{\mathbf{u}} + \int_{V_0} \delta\mathbf{E}^{\mathrm{T}}\mathbf{S}\,\mathrm{d}V - \delta\mathbf{u}^{\mathrm{T}}\mathbf{F}_{\mathrm{ext}} - \delta\mathbf{u}^{\mathrm{T}}\mathbf{R} \tag{27}$$

has to vanish for every virtual displacement $\delta\mathbf{u}$. In Eq. (27), V_0 is the domain of the initial configuration, $\mathbf{F}_{\mathrm{ext}}$ the vector of external loads, $\mathbf{R}$ the contact reaction vector, $\mathbf{M}$ the mass matrix, $\mathbf{A}$ the damping matrix, $\dot{\mathbf{u}}$ the velocity vector and $\ddot{\mathbf{u}}$ the acceleration vector. In view of Eqs. (22) and (26), it comes

$$\delta\mathbf{S} = \mathbf{D}\delta\mathbf{E} = \mathbf{D}\big(\mathbf{B}_L + \mathbf{B}_{NL}(\mathbf{u})\big)\delta\mathbf{u} \tag{28}$$

where $\mathbf{D}$ denotes the usual material secant tangent matrix, deduced from the stress–strain tangent operator $\mathbb{D}$ (Eq. (22)) due to its major and minor symmetry.

Substituting $\delta\mathbf{E}$ from Eq. (26), Eq. (27) results in

$$\delta U = \delta\mathbf{u}^{\mathrm{T}}\mathbf{M}\ddot{\mathbf{u}} + \delta\mathbf{u}^{\mathrm{T}}\mathbf{A}\dot{\mathbf{u}} + \delta\mathbf{u}^{\mathrm{T}}\int_{V_0} \big(\mathbf{B}_L + \mathbf{B}_{NL}(\mathbf{u})\big)^{\mathrm{T}}\mathbf{S}\,\mathrm{d}V - \delta\mathbf{u}^{\mathrm{T}}\mathbf{F}_{\mathrm{ext}} - \delta\mathbf{u}^{\mathrm{T}}\mathbf{R} \tag{29}$$

The vector of internal forces is defined by

$$\mathbf{F}_{\mathrm{int}} = \int_{V_0} \big(\mathbf{B}_L + \mathbf{B}_{NL}(\mathbf{u})\big)^{\mathrm{T}}\mathbf{S}\,\mathrm{d}V \tag{30}$$

Since $\delta\mathbf{u}$ is arbitrary, the following set of nonlinear equations is obtained:

$$\mathbf{M}\ddot{\mathbf{u}} + \mathbf{A}\dot{\mathbf{u}} + \mathbf{F}_{\mathrm{int}} - \mathbf{F}_{\mathrm{ext}} - \mathbf{R} = 0 \tag{31}$$

It is remarked that the stiffness effect is taken into account through the internal forces vector $\mathbf{F}_{\mathrm{int}}$. Eq. (31) can be transformed to

$$\mathbf{M}\ddot{\mathbf{u}} = \mathbf{F} + \mathbf{R}, \qquad \mathbf{F} = \mathbf{F}_{\mathrm{ext}} - \mathbf{F}_{\mathrm{int}} - \mathbf{A}\dot{\mathbf{u}} \tag{32}$$

to be solved with the initial conditions at $t = 0$,

$$\dot{\mathbf{u}} = \dot{\mathbf{u}}_0 \quad \text{and} \quad \mathbf{u} = \mathbf{u}_0 \tag{33}$$

Taking the derivative of $\mathbf{F}_{\mathrm{int}}$ with respect to the nodal displacements $\mathbf{u}$ yields the tangent stiffness matrix:

$$\mathbf{K} = \frac{\partial\mathbf{F}_{\mathrm{int}}}{\partial\mathbf{u}} = \mathbf{K}_e + \mathbf{K}_\sigma + \mathbf{K}_u \tag{34}$$

where $\mathbf{K}_e$, $\mathbf{K}_\sigma$ and $\mathbf{K}_u$ stand respectively for the elastic stiffness matrix, the geometric stiffness (or initial stress stiffness) matrix and the initial displacement stiffness matrix:

$$\mathbf{K}_e = \int_{V_0} \mathbf{B}_L^{\mathrm{T}}\mathbf{D}\mathbf{B}_L\,\mathrm{d}V \tag{35}$$

$$\mathbf{K}_\sigma = \int_{V_0} \frac{\partial\mathbf{B}_{NL}^{\mathrm{T}}}{\partial\mathbf{u}}\mathbf{S}\,\mathrm{d}V \tag{36}$$

$$\mathbf{K}_u = \int_{V_0} \big(\mathbf{B}_L^{\mathrm{T}}\mathbf{D}\mathbf{B}_{NL} + \mathbf{B}_{NL}^{\mathrm{T}}\mathbf{D}\mathbf{B}_L + \mathbf{B}_{NL}^{\mathrm{T}}\mathbf{D}\mathbf{B}_{NL}\big)\,\mathrm{d}V \tag{37}$$

3.2. First-order time integration

Eq. (32) has to be integrated between consecutive time configurations at time t and $t + \Delta t$. Usually a Newmark scheme based on a second-order approximation is used. However, in impact problems, this scheme may lead to no physical energy blow-up as shown in [5]. At the moment of a sudden change of contact conditions (impact, release of contact), the velocity and acceleration are not continuous in time, and excessive regularity of constraints may lead to errors. For this reason, Jean [9] proposed a first-order time scheme which is used in this work. This scheme is based on the following approximations:

$$\int_t^{t+\Delta t} \mathbf{M}\,\mathrm{d}\dot{\mathbf{u}} = \mathbf{M}\big(\dot{\mathbf{u}}^{t+\Delta t} - \dot{\mathbf{u}}^t\big) \tag{38}$$

$$\int_t^{t+\Delta t} \mathbf{F}\,\mathrm{d}t = \Delta t\big((1-\xi)\mathbf{F}^t + \xi\mathbf{F}^{t+\Delta t}\big) \tag{39}$$

$$\int_t^{t+\Delta t} \mathbf{R}\,\mathrm{d}t = \Delta t\mathbf{R}^{t+\Delta t} \tag{40}$$

$$\mathbf{u}^{t+\Delta t} - \mathbf{u}^t = \Delta t\big((1-\theta)\dot{\mathbf{u}}^t + \theta\dot{\mathbf{u}}^{t+\Delta t}\big) \tag{41}$$

with the parameters $0 \leqslant \xi,\ \theta \leqslant 1$. In the iterative solution procedure, all the values at time $t + \Delta t$ are replaced by the values of the current iteration $i + 1$; for example, $\mathbf{F}^{t+\Delta t} = \mathbf{F}^{i+1}$. A standard approximation of $\mathbf{F}^{i+1}$ is

$$\mathbf{F}^{i+1} = \mathbf{F}^i_{\text{int}} + \frac{\partial\mathbf{F}}{\partial\mathbf{u}}\big(\mathbf{u}^{i+1} - \mathbf{u}^i\big) + \frac{\partial\mathbf{F}}{\partial\dot{\mathbf{u}}}\big(\dot{\mathbf{u}}^{i+1} - \dot{\mathbf{u}}^i\big) = \mathbf{F}^i_{\text{int}} - \mathbf{K}^i\Delta\mathbf{u} - \mathbf{A}^i\Delta\dot{\mathbf{u}} \tag{42}$$

Finally, we obtain the recursive form of Eq. (32) in terms of displacements:

$$\begin{aligned}&\bar{\mathbf{K}}^i\Delta\mathbf{u} = \bar{\mathbf{F}}^i + \bar{\mathbf{F}}^i_{\text{acc}} + \mathbf{R}^{i+1}\\ &\mathbf{u}^{i+1} = \mathbf{u}^i + \Delta\mathbf{u}\end{aligned} \tag{43}$$

where the so-called effective terms are given by

$$\bar{\mathbf{K}}^i = \xi\mathbf{K}^i + \frac{\xi}{\theta\Delta t}\mathbf{A}^i + \frac{1}{\theta\Delta t^2}\mathbf{M}^i \tag{44}$$

$$\bar{\mathbf{F}}^i_{\text{acc}} = -\frac{1}{\theta\Delta t^2}\mathbf{M}^i\{\mathbf{u}^i - \mathbf{u}^t - \Delta t\dot{\mathbf{u}}^t\} \tag{45}$$

$$\bar{\mathbf{F}}^i = (1-\xi)\big(\mathbf{F}^t_{\text{int}} + \mathbf{F}^t_{\text{ext}}\big) + \xi\big(\mathbf{F}^i_{\text{int}} + \mathbf{F}^{t+\Delta t}_{\text{ext}}\big) \tag{46}$$

To complete the time step, the velocity is updated according to

$$\dot{\mathbf{u}}^{t+\Delta t} = \left(1 - \frac{1}{\theta}\right)\dot{\mathbf{u}}^t + \frac{1}{\theta\Delta t}\big(\mathbf{u}^{t+\Delta t} - \mathbf{u}^t\big) \tag{47}$$

Eq. (43) is strongly nonlinear, because of large rotations and large deformations involved. Besides, in multibody contact/impact problems, unilateral contact and friction, characterized by inequalities, are non-smooth phenomena. To solve this equation instead of considering all nonlinearities at the same time, a strategy was proposed in [26] which consists in separating the nonlinearities so as to overcome the complexity of calculation and to improve the numerical stability. As $\Delta\mathbf{u}$ and $\mathbf{R}$ are both unknown, Eq. (43) cannot be directly solved. First, the vector $\mathbf{R}$ is determined using the bi-potential method in a reduced system, involving only contact nodes. The reader can refer to [6,7,26,27] for more details on the bi-potential method. Then, the vector $\Delta\mathbf{u}$ is computed over the whole structure, using contact reactions as external loadings. It is important to note that, as opposed to the penalty method or Lagrange multiplier method, the bi-potential method neither changes the global stiffness matrix nor increases the number of degrees of freedom. This interesting feature makes it easy to implement contact and friction problems in existing general-purpose finite element codes. In addition, the solution procedure is more stable because of the separation of nonlinearities and improved numerical algorithms for calculation of contact reactions.

4. Numerical results

The algorithms presented above have been implemented in the finite element code FER/Impact [28,29]. Many application examples, in static or quasi-static cases, have been carried out using the present method [7,26]. To illustrate the results of the contact/impact simulation using the algorithm described above, we consider here two examples.

4.1. Boussinesq–Love contact problem

We outline the classical approach to finding the stresses and displacements produced in an elastic half-space, bounded by the plane surface $z = 0$, under the action of normal and tangential tractions applied to a closed area S of the surface (Fig. 1). We take $C(\xi, \eta)$ to be a surface point within the loaded area S, whilst $A(x, y, z)$ is a general point within the body of the solid. The distance between C and A is denoted by ρ. Distributions of tractions $q_x(\xi, \eta)$, $q_y(\xi, \eta)$ and $p(\xi, \eta)$ act on the area S.

Boussinesq [22] proposed the following potential functions:

$$F_1 = \int_S q_x(\xi, \eta)\big[z \ln(\rho + z) - \rho\big]\,\mathrm{d}\xi\,\mathrm{d}\eta \tag{48}$$

$$G_1 = \int_S q_y(\xi, \eta)\big[z \ln(\rho + z) - \rho\big]\,\mathrm{d}\xi\,\mathrm{d}\eta \tag{49}$$

$$H_1 = \int_S p(\xi, \eta)\big[z \ln(\rho + z) - \rho\big]\,\mathrm{d}\xi\,\mathrm{d}\eta \tag{50}$$

$$F = \frac{\partial F_1}{\partial z} = \int_S q_x(\xi, \eta) \ln(\rho + z)\,\mathrm{d}\xi\,\mathrm{d}\eta \tag{51}$$

$$G = \frac{\partial G_1}{\partial z} = \int_S q_y(\xi, \eta) \ln(\rho + z)\,\mathrm{d}\xi\,\mathrm{d}\eta \tag{52}$$

$$H = \frac{\partial H_1}{\partial z} = \int_S p(\xi, \eta) \ln(\rho + z)\,\mathrm{d}\xi\,\mathrm{d}\eta \tag{53}$$

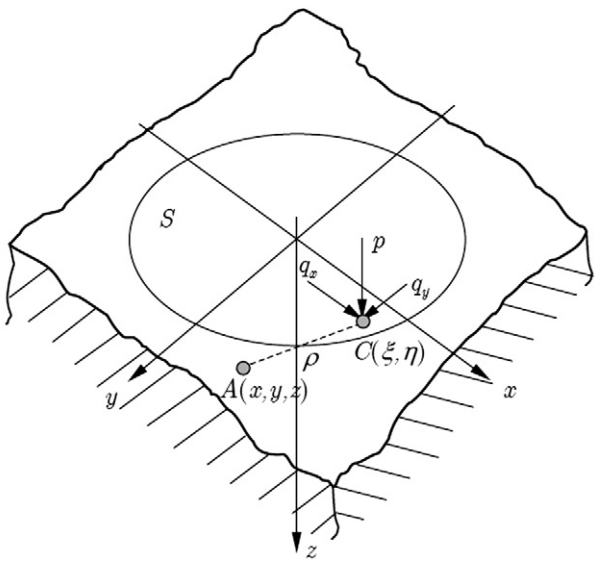

Fig. 1. Loading of an elastic half-space.

Fig. 1. Chargement sur un domaine semi-infini élastique.

$$\psi_1 = \frac{\partial F_1}{\partial x} + \frac{\partial G_1}{\partial y} + \frac{\partial H_1}{\partial z} \tag{54}$$

$$\psi = \frac{\partial F}{\partial x} + \frac{\partial G}{\partial y} + \frac{\partial H}{\partial z} \tag{55}$$

It is noted that ψ_1 and ψ are harmonic functions of x, y and z, i.e. they both satisfy Laplace's equation,

$$\nabla^2\psi_1 = 0, \qquad \nabla^2\psi = 0 \tag{56}$$

Love [24] showed that the components of elastic displacement u_x, u_y and u_z at any point A in the solid can be expressed in terms of the above functions as follows:

$$u_x = \frac{1+\nu}{2\pi E}\left(2\frac{\partial F}{\partial z} - \frac{\partial H}{\partial x} + 2\nu\frac{\partial \psi_1}{\partial x} - z\frac{\partial \psi}{\partial x}\right) \tag{57}$$

$$u_y = \frac{1+\nu}{2\pi E}\left(2\frac{\partial G}{\partial z} - \frac{\partial H}{\partial y} + 2\nu\frac{\partial \psi_1}{\partial y} - z\frac{\partial \psi}{\partial y}\right) \tag{58}$$

$$u_z = \frac{1+\nu}{2\pi E}\left(\frac{\partial H}{\partial z} + (1-2\nu)\psi - z\frac{\partial \psi}{\partial z}\right) \tag{59}$$

where E and ν are respectively the Young's modulus and Poisson's ratio of the elastic half-space. The displacements having been found, the stresses can be calculated from the corresponding strains by Hooke's law.

Under the action of a purely normal pressure $p(\xi, \eta)$, which would occur in a frictionless contact, the above equations may be simplified ($F_1 = F = G_1 = G = 0$).

We consider now the Boussinesq–Love punching problem which concerns the frictionless contact between a rigid cone and an elastic half-space as shown in Fig. 2.

Based on the Boussinesq's theory of potential, Love [23] evaluated the contact pressure $p(s)$ on the face of the cone and the total contact force P in function of the displacement δ of the cone:

$$p(s) = \frac{E}{2(1-\nu^2)}\cot\alpha\cosh^{-1}\left(\frac{a}{s}\right) \tag{60}$$

$$P = \frac{8E}{\pi(1-\nu^2)}\tan(\alpha)\delta^2 \tag{61}$$

In order to validate the numerical approach we have developed, a finite element model of the Boussinesq–Love contact problem is created by using axisymmetric isoparametric elements. The characteristics of the problem are: $E = 10$ MPa, $\nu = 0.495$, $a_i = 0$ and $\alpha = 60°$. Fig. 3 shows the initial mesh and the deformed shape of the half-space together with the distribution of the von Mises stress. We observe a stress concentration at the tip zone of the cone as predicted by Eq. (60). The maximum value of the von Mises stress is 13.868 MPa. Fig. 4 plots the evolution of the total contact force versus the displacement of the cone. Numerical solution is compared with the analytical one given by Eq. (61).

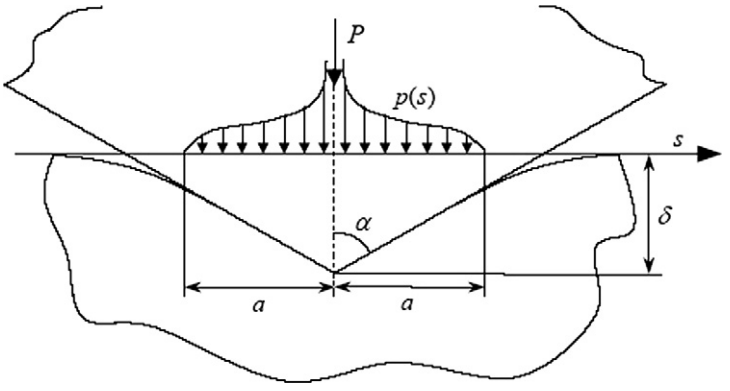

Fig. 2. Boussinesq–Love contact between a rigid cone and an elastic half-space.

Fig. 2. Contact de Boussinesq–Love entre un cône rigide et un domaine semi-infini élastique.

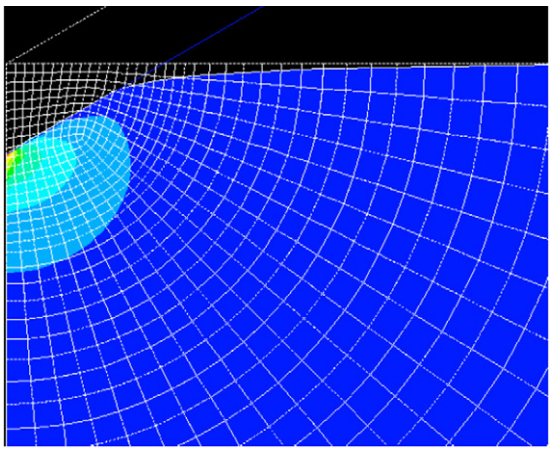

Fig. 3. Deformed mesh with von Mises stress.
Fig. 3. Maillage déformé avec contrainte de von Mises.

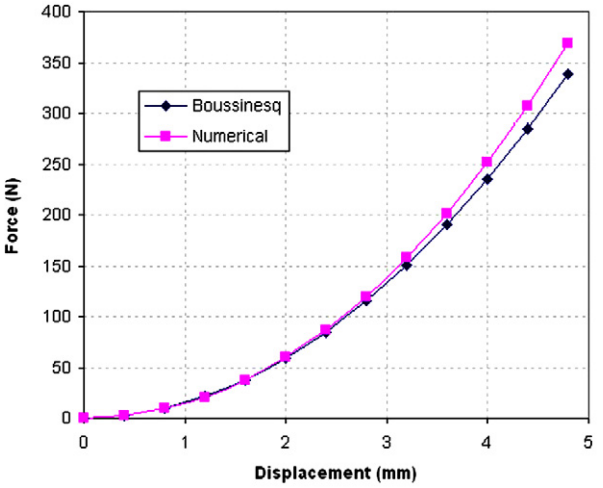

Fig. 4. Load–displacement curve.
Fig. 4. Courbe force–déplacement.

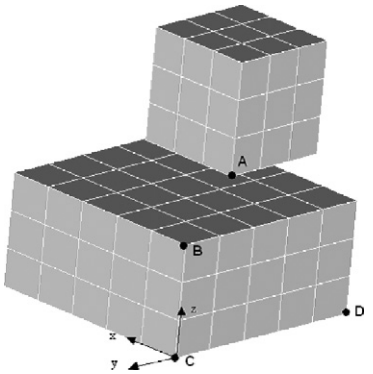

Fig. 5. Initial configuration and mesh.
Fig. 5. Configuration initiale et maillage.

As we can see, when the displacement is relatively small, good concordance is observed between numerical and analytical solutions. However, the difference increases with respect to the displacement. This can be explained by the fact that the analytical solution is determined under the assumption of small deformations. In the numerical algorithm developed above, large deformations are taken into account by means of the calculation of the internal force vector and the tangent stiffness matrix as in Eqs. (30), (34).

4.2. 3D impact problem

This example was initially proposed by Love and Laursen [30] on considering a linear elastic material model. We assume that no damping exists except for Coulomb friction between contact surfaces, i.e. $\mathbf{A}^i = 0$ in Eq. (44). The problem consists in two three-dimensional hyperelastic blocks (Fig. 5) that impact with relative tangential motion. Normalized units are used in this example. The base of the larger block is fixed, and the smaller block has an initial rigid-body velocity of $\{0.0, 1.5, -1.0\}$ that initiates a glancing impact. The larger block initially occupies the cubic space defined by diagonal corner points $\{0, 0, 0\}$ and $\{2.0, 2.0, 1.0\}$ and the smaller block is similarly defined by points $\{0.5, 0.0, 1.25\}$ and $\{1.5, 1.0, 2.25\}$. The density is 100. The initial shear modulus G and bulk modulus K are chosen as in [30]: $G = 5000$, $K = 3333$. Other parameters of the **3é** model are: $a_1 = 50$, $a_2 = 50$, $a_3 = 0$, $a_4 = 2000$ and $a_5 = 100$. The total simulation time is 1 scaled time unit and the numerical parameters are: $\Delta t = 10^{-2}$, $\xi = \theta = 0.5$.

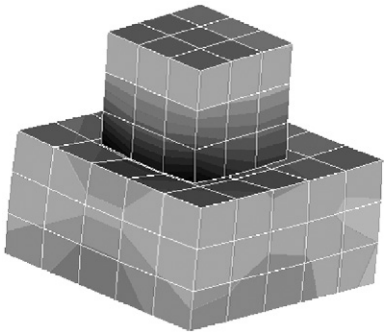

Fig. 6. Deformed shape ($\mu = 0.2$, $t = 0.4$).
Fig. 6. Configuration déformée ($\mu = 0{,}2$, $t = 0{,}4$).

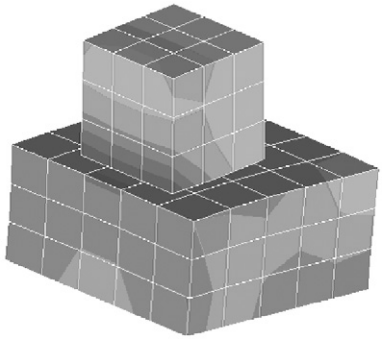

Fig. 7. Deformed shape ($\mu = 0.2$, $t = 0.6$).
Fig. 7. Configuration déformée ($\mu = 0{,}2$, $t = 0{,}6$).

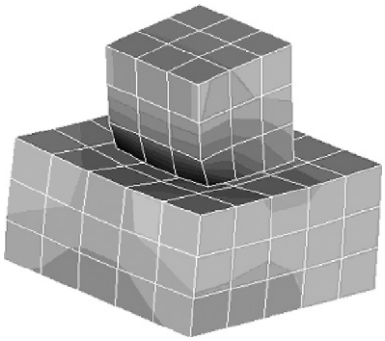

Fig. 8. Deformed shape ($\mu = 0.8$, $t = 0.4$).
Fig. 8. Configuration déformée ($\mu = 0{,}8$, $t = 0{,}4$).

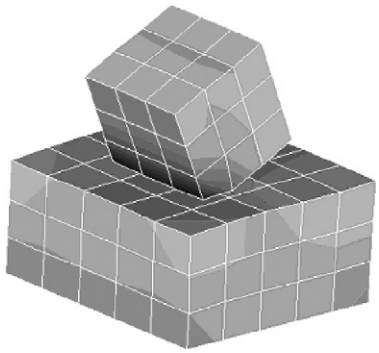

Fig. 9. Deformed shape ($\mu = 0.8$, $t = 0.6$).
Fig. 9. Configuration déformée ($\mu = 0{,}8$, $t = 0{,}6$).

To investigate the frictional effects on the energy dissipation, different coefficients of Coulomb friction are used: $\mu = 0.0$ (frictionless), $0.2, 0.5, 0.8$.

Figs. 6 and 7 show the deformed shapes at time $t = 0.4$ and $t = 0.6$ with the friction coefficient $\mu = 0.2$. The isocontours represent the distribution of the von Mises stress inside the blocks (the maximum value is 1330 unit of stress). Similarly, Figs. 8 and 9 show the case with $\mu = 0.8$. The maximum value of the von Mises stress is 3330 unit of stress. These plots highlight the impact of the friction coefficient on the stress level and relative slips. The case with $\mu = 0.2$ corresponds to a sliding contact status while the case with $\mu = 0.8$ corresponds to almost a sticking contact status. This result is in good agreement with the observation reported by Love and Laursen [30].

Figs. 10–12 show the plots of the kinetic energy E_k, the elastic strain energy E_e and the total energy E_t as a function of time. We observe that the total energy is quite well conserved in the case of frictionless contact (Fig. 12). However, in the case of frictional contact, the total energy decreases. So the total energy is dissipated by frictional effects as expected. It is worth mentioning that the dissipated energy is quantitatively determined.

It is also interesting to examine another question: is the dissipated energy proportional to the friction coefficient? The answer is negative according to numerical results. The proof is illustrated in Fig. 12 where we observe almost the same dissipated energy even for two different friction coefficients ($\mu = 0.2, 0.5$). In addition, the dissipated energy is less for $\mu = 0.8$ than for $\mu = 0.2$ or $\mu = 0.5$. In fact, when the friction coefficient increases, the friction forces increase too. However, the tangential slips decreases. We know that the dissipated energy depends not only on the friction forces but also on the tangential slips on the contact surface.

Figs. 13 and 14 show respectively the evolution of the von Mises stress at point A and σ_{zz} at point C (see Fig. 5). It can be seen that when the friction coefficient increases, the stress level is bigger. The trajectory of point B in the plane BCD (see Fig. 5) is depicted in Fig. 15. We observe that the amplitude of the displacements increases with the friction coefficient as expected.

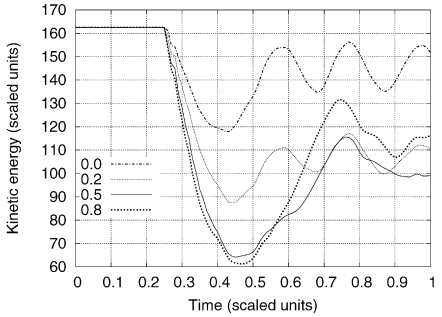

Fig. 10. Kinetic energy with different μ.

Fig. 10. Énergie cinétique avec différent μ.

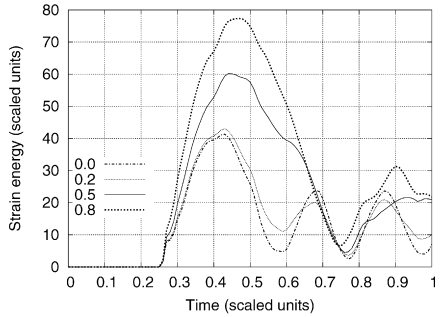

Fig. 11. Strain energy with different μ.

Fig. 11. Énergie de déformation avec différent μ.

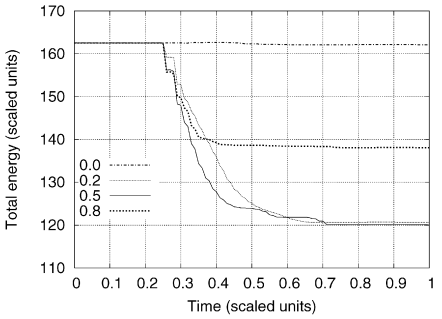

Fig. 12. Total energy with different μ.

Fig. 12. Énergie totale avec différent μ.

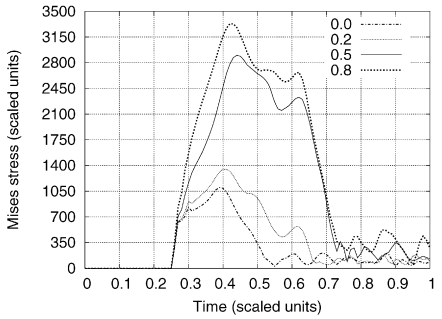

Fig. 13. von Mises stress at point A.

Fig. 13. Contrainte de von Mises au point A.

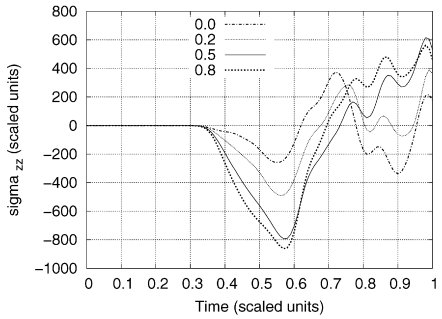

Fig. 14. σ_{zz} at point C.

Fig. 14. σ_{zz} au point C.

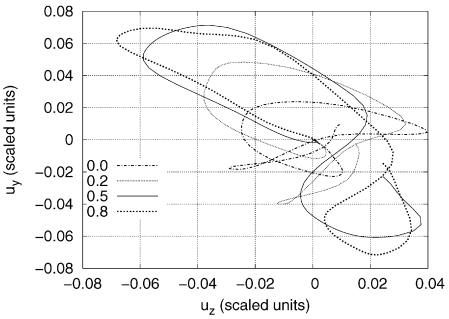

Fig. 15. Trace of point B in the plane BCD.

Fig. 15. Trajectoire du point B dans le plan BCD.

5. Conclusion

In this article, we have proposed a finite element implementation of the **3**é hyperelastic model. The classical Boussinesq–Love contact problem has been treated and numerical solutions are in good concordance with analytical prediction. The classical Boussinesq–Love theory is restricted to frictionless contact and perfectly elastic solids with small deformations. These restrictions are removed in the developed numerical approach. The case of dynamic contact with Coulomb friction between two hyperelastic blocks has also been studied. From numerical experiments on this problem, we have observed that:

– the total energy is well conserved for frictionless contact,
– the algorithm allows to determine quantitatively the physical energy dissipation by friction,

– the dissipated energy is not a monotonic function of the friction coefficient,
– the tumbling behavior is numerically recovered.

References

[1] K.L. Johnson, Contact Mechanics, Cambridge University Press, 1985.
[2] N. Kikuchi, J.T. Oden, Contact Problems in Elasticity: A Study of Variational Inequalities and Finite Elements, SIAM, Philadelphia, 1988.
[3] Z.H. Zhong, Finite Element Procedures in Contact–Impact Problems, Oxford University Press, 1993.
[4] P. Wriggers, Computational Contact Mechanics, John Wiley & Sons, 2002.
[5] T.A. Laursen, Computational Contact and Impact Mechanics: Fundamentals of Modeling Interfacial Phenomena in Nonlinear Finite Element Analysis, Springer-Verlag, 2002.
[6] G. de Saxcé, Z.-Q. Feng, The bi-potential method: a constructive approach to design the complete contact law with friction and improved numerical algorithms, Math. Comput. Modeling 28 (4–8) (1998) 225–245. Special issue: Recent Advances in Contact Mechanics.
[7] Z.-Q. Feng, F. Peyraut, N. Labed, Solution of large deformation contact problems with friction between Blatz–Ko hyperelastic bodies, Int. J. Engrg. Sci. 41 (2003) 2213–2225.
[8] H.M. Hilber, T.J.R. Hughes, R.L. Taylor, Improved numerical dissipation for the time integration algorithms in structural dynamics, Earthquake Engrg. Struc. Dyn. 5 (1977) 283–292.
[9] M. Jean, The non-smooth contact dynamics method, Comp. Meth. Appl. Mech. Engrg. 177 (1999) 235–257.
[10] Z.-Q. Feng, B. Magnain, J.-M. Cros, P. Joli, Energy dissipation by friction in dynamic multibody contact problems, in: Z.-H. Yao, M.-W. Yuan, W.-X. Zhong (Eds.), Computational Mechanics, Beijing, China, Sept. 2004, WCCM VI in conjunction with APCOM04, Springer.
[11] Z.-Q. Feng, F. Peyraut, Q.-C. He, Finite deformations of Ogden's materials under impact loading, Int. J. Non-Linear Mech. 41 (2006) 575–585.
[12] B. Magnain, Développement d'algorithmes et d'un code de calcul pour l'étude des problèmes de l'impact et du choc, PhD thesis, Université d'Evry – Val d'Essonne, 2006.
[13] P.A. Du Bois, S. Kolling, W. Fassnacht, Modelling of safety glass for crash simulation, Comput. Mater. Sci. 28 (2003) 675–683.
[14] P.J. Blatz, W.L. Ko, Application of finite elastic theory to the deformation of rubbery materials, Trans. Soc. Rheology 6 (1962) 223–251.
[15] R.W. Ogden, Non-Linear Elastic Deformations, Ellis Horwood, 1984.
[16] P.G. Ciarlet, Elasticité Tridimensionnelle, Collection RMA, Masson, 1985.
[17] E.M. Arruda, M.C. Boyce, A three dimensional constitutive model for the large deformation stretch behavior of rubber elastic materials, J. Mech. Phys. Solids 41 (1993) 389–412.
[18] A.N. Gent, A new constitutive relation for rubber, Rubber Chem. Technol. 69 (1996) 59–61.
[19] J.C. Simo, T.J.R. Hughes, Computational Inelasticity, Springer-Verlag, New York, 1998.
[20] C.O. Horgan, G. Saccomandi, Finite thermoelasticity with limiting chain extensibility, J. Mech. Phys. Solids 51 (2003) 1127–1146.
[21] E. Lainé, C. Vallée, D. Fortuné, Nonlinear isotropic constitutive laws: choice of the three invariants, convex potentials and constitutive inequalities, Int. J. Engrg. Sci. 37 (1999) 1927–1941.
[22] J. Boussinesq, Application des potentiels à l'étude de l'équilibre et du mouvement des solides élastiques, Gauthier–Villars, Paris, 1885.
[23] A.E.H. Love, Boussinesq's problem for a rigid cone, Quart. J. Math. 10 (1939) 161.
[24] A.E.H. Love, A Treatise on the Mathematical Theory of Elasticity, University Press, Cambridge, 1952.
[25] J.C. Criscione, Rivlin's representation formula is ill-conceived for the determination of response functions via biaxial testing, J. Elasticity 70 (2003) 129–147.
[26] Z.-Q. Feng, 2D or 3D frictional contact algorithms and applications in a large deformation context, Comm. Numer. Meth. Engrg. 11 (1995) 409–416.
[27] G. de Saxcé, Z.-Q. Feng, New inequality and functional for contact with friction: The implicit standard material approach, Mech. Struct. Mach. 19 (1991) 301–325.
[28] Z.-Q. Feng, B. Magnain, J.-M. Cros, FER/impact: Logiciel de simulation numérique des problèmes d'impact, Rev. Europ. Mécanique Numérique 15 (2006) 175–186.
[29] Z.-Q. Feng, http://gmfe16.cemif.univ-evry.fr:8080/~feng/FerImpact.html.
[30] G.R. Love, T.A. Laursen, Improved implicit integrators for transient impact problems: dynamic frictional dissipation within an admissible conserving framework, Comp. Meth. Appl. Mech. Engrg. 192 (2003) 2223–2248.